Revealing Urban–Rural Disparities in Pre-Event Planning for Distribution Network Resilience under Coupled Wind–Rainfall Hazards

Shuo Li[†‡], Dong Liu[§], and Chi K. Tse[†], Shouxiang Wang[‡] and Qianyu Zhao[‡]
[†]Department of Electrical Engineering, City University of Hong Kong, Hong Kong
[‡]State key laboratory of Smart Power Distribution Equipment and System, Tianjin University, Tianjin, China
[§]School of Science and Technology, Hong Kong Metropolitan University, Hong Kong SAR, China
Email: sli566-c@my.cityu.edu.hk, adliu@hkmu.edu.hk, chitse@cityu.edu.hk, {sxwang, zhaoqianyu}@tju.edu.cn

***Abstract*—Extreme hurricanes combining high winds and heavy rainfall increasingly threaten power distribution networks. Existing pre-event planning is largely wind-centric and based on stylized test systems, overlooking urban–rural differences and flood exposure. This paper presents a scenario-based framework integrating coupled wind–rainfall modeling, component fragility, and workload-aware preparedness optimization. Case studies on two realistic Virginia networks, including urban Colonial Heights and rural Richmond County, show that coupling hazards raises peak failure risk by 54.8% in the urban system but only 5.7% in the rural system, and extends recovery duration. Optimal strategies diverge: urban areas shift from line hardening to flood protection, while rural systems emphasize vegetation management. With identical resources, event load-loss reductions reach 58.5% (urban) and 21.4% (rural). Results highlight that explicitly modeling flood impacts and aligning preparedness with network typology significantly enhance resilience and provide actionable guidance for utility decision-making.**

***Index Terms*—Distribution networks, Extreme weather events, Pre-event preparedness, Urban-rural disparities, Wind-rainfall hazards**

I. Introduction

Extreme weather events, particularly hurricanes, pose escalating threats to power distribution networks under a warming climate. From 2000 to 2023, weather-related disturbances accounted for roughly 80% of major U.S. outages, with hurricanes causing the most widespread and prolonged blackouts [1]. While long-term infrastructure upgrades remain essential, pre-event planning provides a cost-effective and rapidly deployable pathway to mitigate hurricane impacts without substantial capital expenditure.

Effective preparedness depends on accurate hazard assessment and the strategic allocation of limited resources to vulnerable components [2]. Existing hurricane impact models, however, are largely wind-centric, focusing on estimating wind fields or statistical wind speed distributions across network footprints [3]. Grid-based parametric wind models estimate wind speed distributions over geographic cells, offering computational efficiency but potentially mischaracterizing storm structures when extrapolated beyond historical calibration [4], [5]. This perspective overlooks rainfall-induced flooding, which can severely damage substations, underground cables, and access roads. Consistently, climate projections indicate a 14% increase in rainfall within 100 km of storm centers under 2 °C global warming [6]. These trends underscore the necessity of modeling coupled wind–rainfall dynamics to enable comprehensive resilience planning.

Pre-event strategies such as mobile generator deployment and targeted hardening [7], [8] are commonly evaluated using IEEE standard test systems. However, these stylized networks fail to capture the inherent heterogeneity of real-world distribution systems. In particular, rural networks, characterized by dispersed loads and extended feeders, exhibit distinct vulnerability patterns and protection priorities compared with compact urban systems [9]. As a result, applying uniform preparedness strategies across heterogeneous networks may lead to inefficient resource allocation and suboptimal resilience enhancement [10], [11].

This paper develops a comprehensive pre-event planning framework that explicitly addresses coupled wind–rainfall hazards across both urban and rural distribution networks. By analyzing realistic network topologies, the study reveals how the effectiveness and prioritization of defense measures vary between system types, thereby offering utilities actionable insights for targeted preparedness. The remainder of this paper is organized as follows. Section II presents the coupled hazard modeling. Section III formulates the pre-event planning optimization model. Section IV reports case studies contrasting urban–rural resilience strategies. Section V concludes with key findings and future research directions.

II. Model for Coupled Wind–Rainfall Hazard

The section first constructs spatiotemporal hurricane hazard fields based on wind and precipitation models. It then quantifies component-level vulnerability to wind and flooding and, finally, develops a stochastic scenario generation and reduction framework for subsequent optimization.

A. Spatiotemporal Hurricane Hazard Field Modeling

Hurricane track data are obtained from NOAA's IBTrACS database [12] and resampled to 30-minute intervals for dynamic distribution network simulations.

979-8-3315-8138-1

The Holland wind field model [13] characterizes gradient wind speed $V(r)$ as a function of radial distance r from the storm center:

$$V(r) = V_m \left[\left(\frac{r_m}{r}\right)^B \exp\left(1 - \left(\frac{r_m}{r}\right)^B\right) \right]^{1/2} \quad (1)$$

where B is a shape parameter governing wind decay rate. This parametric representation provides computationally efficient wind field estimation while maintaining sufficient accuracy for power system applications.

Rainfall modeling employs the R-CLIPER statistical framework [14], which assumes a radially symmetric precipitation distribution. The radial precipitation profile $P(r)$ follows:

$$P(r) = \begin{cases} T_0 + (T_m - T_0)\frac{r}{r_p} & \text{for } r \leq r_p \\ T_m \exp\left(-\frac{r - r_p}{r_e}\right) & \text{for } r > r_p \end{cases} \quad (2)$$

where T_0 and T_m denote precipitation rates at the storm center and maximum, respectively, r_p defines the inner-core radius, and r_e characterizes the outer rain field extent.

B. Component Vulnerability and Failure Modeling

Distribution network components exhibit distinct vulnerability characteristics depending on their installation configurations. Overhead lines primarily fail under wind-induced mechanical stress, whereas underground components including substations and cable terminals, are more vulnerable to flood-induced submersion. This installation-dependent behavior necessitates differentiated hazard–exposure relationships in modeling distribution system failures.

Rainfall-to-flood conversion is represented by a parameterized hydrological function [15], which relates flood depth h (m) to rainfall intensity r (mm/h) through terrain-dependent coefficients:

$$h = f(r) = a_3 r^3 + a_2 r^2 + a_1 r + a_0 \quad (3)$$

with empirically calibrated parameters $a_3 = 5.806 \times 10^{-8}$, $a_2 = -5.458 \times 10^{-5}$, $a_1 = 0.01795$, and $a_0 = -0.3911$.

Component failure probabilities are estimated using lognormal fragility functions derived from historical outage data:

$$P(\text{failure}|w) = \Phi\left[\frac{1}{\beta}(\ln w - \lambda)\right] \quad (4)$$

where w denotes the local hazard intensity, $\Phi(\cdot)$ is the standard normal cumulative distribution function (CDF), and (β, λ) are the distribution parameters. Fragility parameters for overhead distribution lines under gust winds (mph) are adopted from Xu *et al.* [16], calibrated using observed outage data and high-resolution wind fields for Hurricane Fiona in Puerto Rico. When local outage and hazard data are available, recalibration of the fragility function is recommended to better reflect region-specific conditions. Fragility parameters for underground components under flood conditions (m) follow Kabre *et al.* [17].

C. Scenario Generation and Reduction Framework

Traditional Sequential Monte Carlo (SMC) simulations often suffer from temporal accumulation bias, which can lead to overestimated failure frequencies during prolonged hazard exposure. To address this limitation, we adopt the Hazard Resistance–Based Spatiotemporal Risk Analysis (HRSRA) framework [16], which assigns time-invariant resistance thresholds R_{ij}^H to each network component via inverse transform sampling:

$$R_{ij}^w = \exp\left(\lambda + \beta \cdot \Phi^{-1}(r_{ij})\right), ij \in \mathcal{L} \quad (5)$$

where $r_{ij} \sim U(0,1)$ and $\mathcal{L}$ denotes the line set. Component ij fails when local hazard intensity exceeds R_{ij}^H, eliminating time-dependency bias.

For each hurricane scenario h, 1,000 HRSRA realizations are generated and reduced to a representative scenario using the method in Li *et al.* [18]. Candidate subsets are evaluated by computing the weighted critical load loss $P_{h,s}^{\text{shed}}$ under the optimal emergency response strategy.

III. Pre-Event Planning Optimization Framework

This section first characterizes preparedness strategy workloads, including resource, logistics, and operational requirements, and then formulates the optimization model that determines cost-effective actions for enhancing distribution network resilience under coupled wind–rainfall hazards.

A. Preparedness Strategy Workload Characterization

Preparedness strategies are distinguished by asset type. Overhead systems include emergency tree trimming (ETT) and emergency line reinforcement (ELR); underground systems adopt emergency flood protection (EFP); and mobile emergency generators (EGs) support post-event restoration.

ETT workloads depend on vegetation density along distribution corridors, typically following roadways. Based on Smart *et al.* [19], urban areas average 1.5 trees/100 m, while rural corridors reach 3.1 trees/100 m [20]. Field practice indicates 0.75 work hours per tree for trimming [21]. For ELR, EPRI guidelines specify 3.1 work hours per utility pole for wind-hardening [22]. For EFP, temporary flood-barrier deployment requires 8 work hours per 100 m segment [23]. These coefficients provide a consistent basis for labor and resource accounting across system types, supporting quantitative workload inputs for the optimization model.

B. Optimization Model Formulation

We formulate a scenario-based pre-event optimization over decisions $\mathbf{R}$: generator placement e_i, reinforcement indicators α_{ij}, trimming indicators β_{ij}, and flood-protection indicators c_{ij}. The objective minimizes expected load not served:

$$\min \sum_t \sum_{i \in \mathcal{N}} (1 - \delta_{i,t}) \cdot P_{i,t}^{\text{L}} \quad (6)$$

where $\mathcal{N}$ is the node set, $P_{i,t}^{\text{L}}$ is the demand at node i and time t, and $\delta_{i,t} \in \{0, 1\}$ is a load shedding indicator, which equals 0 if the load at node i is shed at time t, and 1 otherwise.

979-8-3315-8138-1

Constraints fall into three groups. First, resource and workload budgets:

$$\sum_{i\in N} e_i \leq E_{\max}, \tag{7}$$

$$\sum_{(i,j)\in\mathcal{L}_{\mathrm{oh}}} \left(\alpha_{ij}k^{\mathrm{ELR}} + \beta_{ij}k^{\mathrm{ETT}}\right) l_{ij} + \sum_{(i,j)\in\mathcal{L}_{\mathrm{ug}}} c_{ij}k^{\mathrm{EFP}} l_{ij} \leq K \tag{8}$$

where $E_{\max}$ is the available number of EGs; l_{ij} is line length (km); k^{ELR}, k^{ETT}, and k^{EFP} are per-length workloads; and K is the total person-hour budget.

Second, hazard-preparedness linkage. ELR and EFP are assumed to fully prevent hurricane-induced failures on treated lines. This is a modeling approximation adopted for optimization convenience and computational tractability. ETT increases wind resistance; empirical evidence suggests a 30% enhancement after trimming [24]. Accordingly, the 30% improvement is treated as a reasonable planning-level approximation. We encode these effects via:

$$u_{ij} \leq \tau_{ij} + \alpha_{ij} - (\tau_{ij}\cdot\alpha_{ij}), \forall (i,j)\in\mathcal{L}_{oh} \tag{9}$$

$$u_{ij} \leq \tau_{ij} + c_{ij} - (\tau_{ij}\cdot c_{ij}), \forall (i,j)\in\mathcal{L}_{ug} \tag{10}$$

$$u_{ij} \leq \tau_{ij} + \beta_{ij}\cdot\rho_{ij} - (\tau_{ij}\cdot\beta_{ij}\cdot\rho_{ij}), \forall (i,j)\in\mathcal{L}_{oh} \tag{11}$$

where $\rho_{ij} = 1$ if the enhanced resistance R^w_{ij} after ETT can withstand scenario hazard w^h_{ij}, and 0 otherwise; $\tau_{ij} = 0$ denotes outage and u_{ij} is the line switching state.

Third, operational constraints for post-event reconfiguration and islanding:

$$\sum_{\{j|j\in\mathcal{L}_{\mathcal{R}_i^{up}}\}} P_{ij,t} - \sum_{\{j|j\in\mathcal{L}_{\mathcal{R}_i^{dn}}\}} P_{ij,t} + \sum_{\{j|j<i,(i,j)\in\mathcal{L}_{\mathcal{T}}\}} P_{ij,t} - \sum_{\{j|i<j,(i,j)\in\mathcal{L}_{\mathcal{T}}\}} P_{ij,t} = \delta_{i,t}\cdot P^L_{i,t} - P^{EG}_{i,t} \tag{12}$$

$$-u_{ij,t}\overline{P}_{ij} \leq P_{ij,t} \leq u_{ij,t}\overline{P}_{ij}, \quad \forall (i,j)\in\mathcal{L} \tag{13}$$

$$\delta_{i,t} \leq h_{i,t}, \forall i\in\mathcal{N} \tag{14}$$

$$\left(\sum_{\{j|j\in\mathcal{RL}_i^{dn}\}} h_{j,t}u_{ij,t} + \sum_{\{j|j\in\mathcal{RL}_i^{up}\}} h_{j,t}u_{ij,t}\right) / |\mathcal{L}_i| \leq h_{i,t} \leq \sum_{\{j|j\in\mathcal{RL}_i^{dn}\}} h_{j,t}u_{ij,t} + \sum_{\{j|j\in\mathcal{RL}_i^{up}\}} h_{j,t}u_{ji,t}, \forall i\in\mathcal{N} \tag{15}$$

$$-M(1-u_{ij,t}) + \frac{(r_{ij}P_{ij,t} + x_{ij}Q_{ij,t})}{V_0} \leq V_{i,t} - V_{j,t} \leq M(1-u_{ij,t}) + \frac{(r_{ij}P_{ij,t} + x_{ij}Q_{ij,t})}{V_0}, \forall (i,j)\in\mathcal{L} \tag{16}$$

$$\underline{V_i} \leq V_{i,t} \leq \overline{V}_i, \forall i\in\mathcal{N} \tag{17}$$

Here, $\mathcal{S}\subseteq\mathcal{N}$ denotes substations; $\mathcal{L}_{\mathcal{R}}$ and $\mathcal{L}_{\mathcal{T}}$ denote regular and tie-lines, respectively; $h_{i,t}$ is the node-energization binary; $P_{ij,t}$ is active power flow with limit $\overline{P}_{ij}$; $V_{i,t}$ is squared voltage magnitude; r_{ij} and x_{ij} are line parameters; and V_0 is the base voltage. Constraint (12) enforces nodal balance; (13) imposes flow limits conditioned on switching; (14) forbids serving de-energized loads; (15) applies power outage logic in distribution networks by relating node energization indicator $h_{i,t}$ to connected line status; (16) applies linearized DistFlow; and (17) enforces voltage bounds. Radiality is ensured via density-based constraints that preclude cycles [25]. This optimization is formulated as a MILP and solved with Gurobi on Ubuntu 22.04.3 LTS with two AMD EPYC 7H12 64-Core CPUs and 512 GB memory.

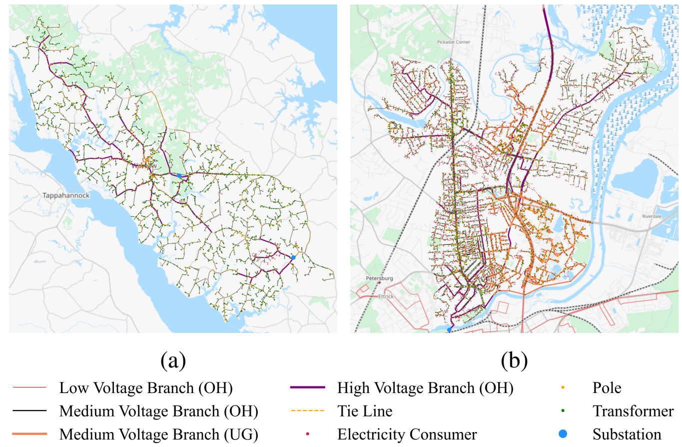

Fig. 1: Real-world distribution network topologies: (a) Richmond and (b) Colonial Heights.

TABLE I. Real-world distribution network parameters and configurations.

City	Nodes	Edges	Underground Rate
Richmond	7854	7872	3.7%
Colonial Heights	13,194	13,242	30.6%

IV. Case Study

To evaluate differences in pre-event planning strategies between urban and rural distribution networks under hurricane hazards, we consider two representative systems in Virginia, USA: a rural network in Richmond County and an urban network in Colonial Heights City. Network topologies are synthesized using the framework in [18], producing realistic infrastructure configurations that reflect distinct geographic and demographic conditions.

The underground distribution penetration for each system is estimated following the approach in [26]. The resulting network compositions align with local socioeconomic and land-use characteristics, providing a representative urban–rural comparison. Key network parameters are summarized in Table I, and the corresponding topological layouts are illustrated in Fig. 1.

For hazard simulation, we adopt Hurricane Floyd (1999) as the representative event, due to its severe impacts in Virginia and its characteristic coupled wind–rainfall profile—strong winds combined with prolonged heavy precipitation that resulted in widespread flooding [27]. The historical storm track is shown in Fig. 2, serving as the spatiotemporal basis for generating wind and rainfall fields used in the scenario analysis.

979-8-3315-8138-1

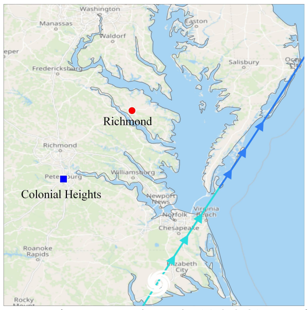

Fig. 2: Hurricane Floyd (1999) trajectory.

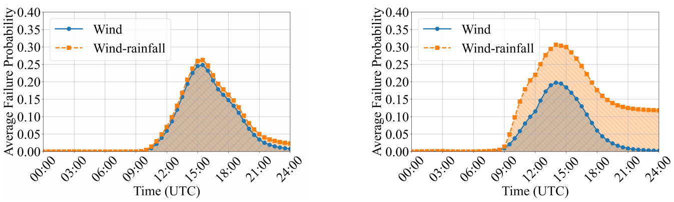

(a) (b)

Fig. 3: Network failure probability evolution: (a) Richmond and (b) Colonial Heights.

A. Evolution of Hurricane Risk for Distribution Networks

Spatiotemporal failure probability analysis reveals distinct vulnerability patterns between rural and urban systems under coupled wind–rainfall hazards. Figure 3 depicts the evolution of network-average failure probabilities throughout the hurricane event, contrasting wind-only and coupled scenarios.

At peak intensity, the rural system experiences only a modest increase (5.7%) in failure probability when transitioning from wind-only to coupled conditions. In contrast, the urban network exhibits a 54.8% increase, reflecting its higher proportion of flood-prone underground assets.

Temporal dynamics also diverge. Under wind-only exposure, failure probabilities decline rapidly after storm passage, consistent with short-lived mechanical impacts. Under coupled hazards, however, elevated urban failure probabilities persist: Colonial Heights retains an 11.8% residual failure probability at the final time step, indicating that flood-induced outages substantially delay system recovery compared with wind-only conditions.

B. Pre-Event Planning Strategies for Distribution Networks

To evaluate preparedness effectiveness, we allocate identical emergency resources to both areas: 120 personnel and 3 mobile emergency power units, with deployment starting five days before landfall. Fig. 4 maps the spatial deployment of measures; Table II quantifies allocation ratios.

Deployment patterns reflect contrasting geography and load density. Mobile units are consistently sited in the town/city center to enable rapid microgrid formation and critical-load restoration. Rural Richmond displays dispersed defenses aligned with distributed loads and lower population density; urban Colonial Heights concentrates resources around high-density districts and critical nodes.

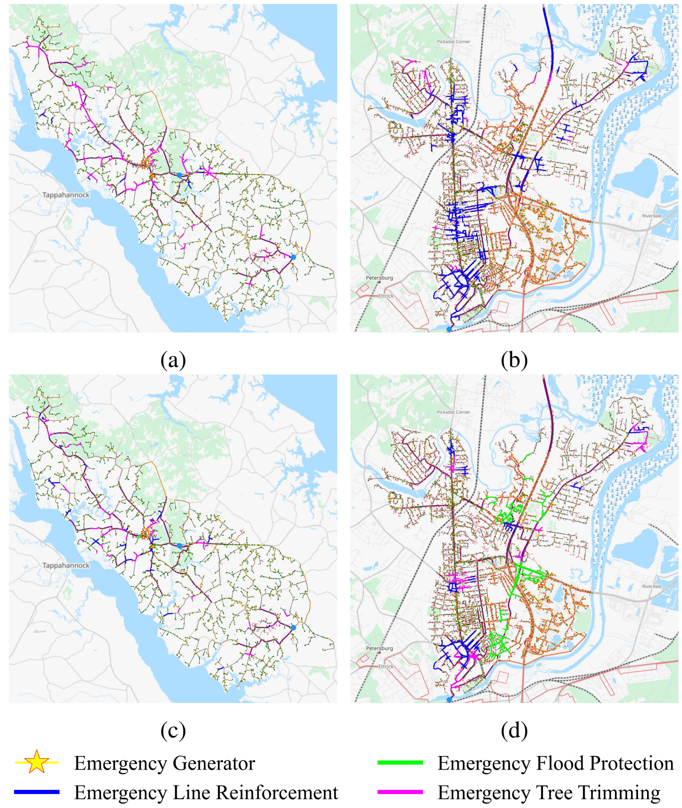

Fig. 4: Spatial deployment of pre-event measures under wind-only (a–b) and coupled wind–rainfall scenarios (c–d).

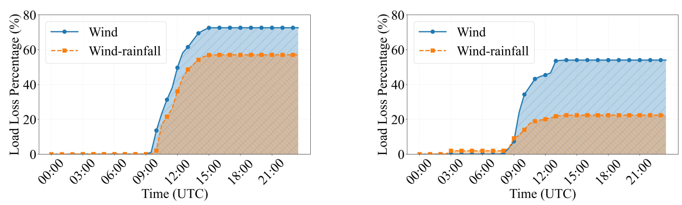

(a) (b)

Fig. 5: Load loss comparison under different scenarios: (a) Richmond and (b) Colonial Heights.

Under wind-only hazards, the urban system prioritizes ELR, allocating 62.68% to line hardening. Under coupled hazards, Colonial Heights markedly shifts: ELR drops to 32.17% while EFP rises to 44.94%, underscoring the need to protect underground infrastructure concentrated in commercial and municipal cores. In contrast, rural Richmond consistently prioritizes ETT—63.05% (wind-only) and 52.46% (coupled). This strategic focus addresses the denser vegetation characteristics of rural environments, where tree-related failures constitute the most common cause of power outages.

Effectiveness is evaluated via load loss during the event (Fig. 5). Despite equal resources, rural systems are harder to defend: under coupled hazards, Richmond achieves a modest 21.39% improvement relative to its wind-only case, whereas Colonial Heights attains a 58.50% improvement. This disparity stems from broader spatial extent and longer feeders in rural

979-8-3315-8138-1

TABLE II. DEFENSE MEASURE ALLOCATION RATIOS UNDER DIFFERENT SCENARIOS.

City	Mode	ELR	EFP	ETT
Richmond	Wind	36.95%	0.00%	63.05%
	Coupled	30.05%	17.49%	52.46%
Colonial Heights	Wind	62.68%	0.00%	37.32%
	Coupled	32.17%	44.94%	22.89%

areas, which dilute efficiency per unit resource and increase time requirements for vegetation management and hardening.

Notably, even though rural failure probabilities differ only slightly between hazard models, neglecting flood protection for limited underground assets in rural town centers still increases load loss by roughly 20%. Targeted EFP therefore remains essential in rural contexts, reinforcing the need to account for coupled hazards regardless of network type.

V. CONCLUSION

This paper developed a comprehensive pre-event planning framework for coupled wind–rainfall hazards in urban and rural distribution networks. The framework integrates spatiotemporal hurricane modeling, installation-dependent component fragility, and a workload-aware optimization of multiple preparedness strategies. Case studies demonstrate clear contrasts between network types: rural systems exhibit lower defense efficiency due to extended feeders and dispersed loads, emphasizing vegetation management, whereas urban systems prioritize flood protection for concentrated underground assets. Explicitly modeling flood effects and aligning preparedness with network typology significantly enhances resilience. Future work will extend these urban–rural findings via multi-scenario stochastic optimization under hurricane uncertainty and benchmark the coupled framework against simplified baselines to quantify marginal resilience gains.

REFERENCES

[1] Climate Central, "Weather-related power outages rising," Apr. 2024, available at: https://www.climatecentral.org/climate-matters/weather-related-power-outages-rising.

[2] Q. Zhang, Z. Wang, S. Ma, and A. Arif, "Stochastic pre-event preparation for enhancing resilience of distribution systems," *Renew. Sustain. Energy Rev.*, vol. 152, p. 111636, 2021.

[3] A. Poudyal, S. Poudel, and A. Dubey, "Risk-based active distribution system planning for resilience against extreme weather events," *IEEE Trans. Sustain. Energy*, vol. 14, no. 2, pp. 1178–1192, 2023.

[4] H. Hou, J. Tang, Z. Zhang, Z. Wang, R. Wei, L. Wang, H. He, and X. Wu, "Resilience enhancement of distribution network under typhoon disaster based on two-stage stochastic programming," *Appl. Energy*, vol. 338, p. 120892, 2023.

[5] H. E. Willoughby and M. E. Rahn, "Parametric representation of the primary hurricane vortex. part i: Observations and evaluation of the holland (1980) model," *Mon. Weather Rev.*, vol. 132, no. 12, pp. 3033–3048, 2004.

[6] Intergovernmental Panel on Climate Change (IPCC), "Weather and climate extreme events in a changing climate," in *Climate Change 2021 – The Physical Science Basis: Working Group I Contribution to the Sixth Assessment Report of the Intergovernmental Panel on Climate Change*. Cambridge: Cambridge University Press, 2023, pp. 1513–1766.

[7] S. Lei, J. Wang, C. Chen, and Y. Hou, "Mobile emergency generator pre-positioning and real-time allocation for resilient response to natural disasters," *IEEE Trans. Smart Grid*, vol. 9, no. 3, pp. 2030–2041, 2018.

[8] Y. Li, S. Lei, W. Sun, C. Hu, and Y. Hou, "A distributionally robust resilience enhancement strategy for distribution networks considering decision-dependent contingencies," *IEEE Trans. Smart Grid*, vol. 15, no. 2, pp. 1450–1465, 2024.

[9] F. Rouhana and J. Zhu, "Examining rural-urban disparity in disaster impact and recovery: Case of tropical storm Isaias," in *Computing in Civil Engineering*, 2023, pp. 219–227.

[10] N. L. Dehghani and A. Shafieezadeh, "Multi-stage resilience management of smart power distribution systems: A stochastic robust optimization model," *IEEE Trans. Smart Grid*, vol. 13, no. 5, pp. 3452–3467, 2022.

[11] S. Ma, L. Su, Z. Wang, F. Qiu, and G. Guo, "Resilience enhancement of distribution grids against extreme weather events," *IEEE Trans. Power Syst.*, vol. 33, no. 5, pp. 4842–4853, 2018.

[12] J. Gahtan, K. R. Knapp, C. J. Schreck, H. J. Diamond, J. P. Kossin, and M. C. Kruk, "International best track archive for climate stewardship (ibtracs) project, version 4r01," https://doi.org/10.25921/82ty-9e16, July 2024, nOAA National Centers for Environmental Information.

[13] G. J. Holland, "An analytic model of the wind and pressure profiles in hurricanes," *Mon. Weather Rev.*, vol. 108, pp. 1212–1218, 1980.

[14] R. E. Tuleya, M. DeMaria, and R. J. Kuligowski, "Evaluation of gfdl and simple statistical model rainfall forecasts for u.s. landfalling tropical storms," *Weather Forecast.*, vol. 22, no. 1, pp. 56–70, 2007.

[15] S. Afzal, H. Mokhlis, H. A. Illias, A. A. Bajwa, H. Mohamad, N. N. Mansor, L. J. Awalin, and A. Ramasamy, "Modeling impact of urban flash floods on power distribution system using monte carlo technique and reinforcement learning," *Ain Shams Eng. J.*, vol. 16, no. 3, p. 103325, 2025.

[16] L. Xu, N. Lin, D. Xi, K. Feng, and H. V. Poor, "Hazard resistance-based spatiotemporal risk analysis for distribution network outages during hurricanes," *IEEE Trans. Power Syst.*, vol. 40, no. 3, pp. 2143–2152, 2025.

[17] W. W. Kabre and M. R. Weimar, "Fragility functions resource report: Documented sources for electricity and water resilience valuation," Pacific Northwest National Laboratory, Richland, WA, Tech. Rep. PNNL-33587, 2022.

[18] S. Li, S. Wang, Q. Zhao, D. Liu, and C. K. Tse, "A risk assessment framework for large-scale synthetic power distribution networks considering historical hurricane disasters," *IEEE Trans. Power Syst.*, vol. 40, no. 5, pp. 3846–3858, 2025.

[19] N. Smart, T. S. Eisenman, and A. Karvonen, "Street tree density and distribution: An international analysis of five capital cities," *Front. Ecol. Evol.*, vol. 8, p. 562646, 2020.

[20] T. Jiang, M. Freudenberg, C. Kleinn, V. Tewari, B. Diwakara, and N. Nölke, "Unveiling urbanization effects on trees outside forests along the urban-rural gradient in megacity bengaluru," *Forest Ecosyst.*, vol. 12, p. 100258, 2025.

[21] D. Bloniarz, H. D. Ryan, C. J. Luley, J. Stratton, and J. Bond, "i-tree storm users manual v4.0," 2024, USDA Forest Service, [Online]. Available: https://www.itreetools.org/documents/253/i-Tree%20Storm%20Users%20Manual.pdf. [Accessed: Aug. 12, 2025].

[22] Electric Power Research Institute, "Epri distribution structural resiliency testing," 2021, [Online]. Available: https://distribution.epri.com/resources/applications/structure-testing/EPRI_Distribution_Structure_Testing.pdf. [Accessed: Aug. 12, 2025].

[23] F. Ogunyoye, R. Stevens, and S. Underwood, "Temporary and demountable flood protection guide," 2011, Environment Agency, [Online]. Available: https://assets.publishing.service.gov.uk/media/603376bce90e0766021bf14f/_flood_protection_guide.pdf. [Accessed: Aug. 12, 2025].

[24] D. Cerrai, P. Watson, and E. N. Anagnostou, "Assessing the effects of a vegetation management standard on distribution grid outage rates," *Electr. Power Syst. Res.*, vol. 175, p. 105909, 2019.

[25] S. Sun, G. Li, C. Chen, Y. Bian, and Z. Bie, "A novel formulation of radiality constraints for resilient reconfiguration of distribution systems," *IEEE Trans. Smart Grid*, vol. 14, no. 2, pp. 1337–1340, 2023.

[26] T. Sun, C. Zanocco, J. Flora, and R. Rajagopal, "Mapping the depths: A stocktake of underground power distribution in United States," in *Proc. IEEE Power & Energy Society General Meeting (PESGM)*, 2024, pp. 1–5.

[27] R. J. Pasch, T. B. Kimberlain, and S. R. Stewart, "Preliminary report: Hurricane floyd," National Hurricane Center, Tech. Rep., 2014. [Online]. Available: https://www.nhc.noaa.gov/data/tcr/AL081999_Floyd.pdf

979-8-3315-8138-1